ELSEVIER

Journal of Alloys and Compounds 452 (2008) 41–47

Journal of ALLOYS AND COMPOUNDS

www.elsevier.com/locate/jallcom

Thermodynamic and kinetic considerations on degradations in solid oxide fuel cell cathodes

Harumi Yokokawa *, Natsuko Sakai, Teruhisa Horita, Katsuhiko Yamaji, M.E. Brito, Haruo Kishimoto

National Institute of Advanced Industrial Science and Technology (AIST), Higashi 1-1-1, AIST Central No. 5, Tsukuba, Ibaraki 305-8565, Japan

Received 18 September 2006; received in revised form 11 December 2006; accepted 13 December 2006
Available online 28 January 2007

Abstract

Analyses have been made to understand the chemical behaviors of the perovskite cathode/rare earth doped ceria interlayer/YSZ (yttria stabilized zirconia) electrolyte multilayer structure and their relation to the electrochemical performance. Particular focus was given to the thermodynamic activities of SrO in the cathodes and their relation to the reaction with rare earth doped ceria or YSZ. The possibility of Sr diffusion from the cathode through the rare earth doped ceria to the YSZ electrolyte to form $SrZrO_3$ was analyzed in terms of the SrO activity. It has been found that the SrO activity at the cathode/ceria interfaces is important for the steepening of the chemical potential gradient of SrO inside the doped ceria and for the enhancement of the solubility of SrO in doped ceria. Two possible effects influencing the SrO activities have been examined; these are chemical reactions between perovskite cathodes and doped ceria and kinetic decomposition under the oxygen potential gradient. Effects of cathodic polarization have been also examined in terms of changes in chemical equilibria and change in oxygen potential gradients.

Keywords: Fuel cells; Oxide materials; Diffusion; Thermochemistry; Degradation; Valence stability; Interface reactions

1. Introduction

Solid oxide fuel cells (SOFC) are expected to have merits of high-energy conversion efficiency and longer life compared with other fuel cells [1,2]. Actually, a seal-less tubular-type SOFC fabricated by the electrochemical vapor deposition (EVD) technique confirmed that good performance has not been degraded for more than 70,000 h at the operation temperature of 1000 °C [3]. In recent years, extensive efforts have been made to lower the operation temperature down to 800 °C. This leads to the surprising achievement that the performance obtained by some intermediate temperature cells around 800 °C is better than that of the high temperature EVD cells around 1000 °C [4,5]. In order to achieve better performance, the followings are usually adopted:

(1) Utilization of metal interconnects instead of oxide interconnects [6]: This will provide a basis for better management of heat and temperature distributions;
(2) Adoption of a thinner electrolyte film to reduce the Ohmic loss [7].
(3) Utilization of cathodes with better performance. Lanthanum strontium ferrite, $(La,Sr)FeO_3$, lanthanum strontium cobaltite, $(La,Sr)CoO_3$, lanthanum strontium cobaltite ferrite, $(La,Sr)(Co,Fe)O_3$, are adopted instead of stable lanthanum strontium manganite, $(La,Sr)MnO_3$ [8].
(4) To avoid chemical reactions [9,10] between the yttria stabilized zirconia (YSZ) electrolyte and such cathodes to form non-conductive $La_2Zr_2O_7$ or $SrZrO_3$, a thin interlayer made of rare earth (typically Gd or Sm) doped ceria is inserted between the cathodes and the YSZ electrolyte. Electrochemical and other investigations on such cathodes with doped ceria electrolyte revealed that the electrode activity is not degraded [11,12], although the same cathode with YSZ electrolyte is known to be degraded [9,10].

On the other hand, adoption of these materials has revealed interesting features associated with degradations of cell performance as follows:

* Corresponding author. Tel.: +81 29 861 4542; fax: +81 29 861 4540.
E-mail address: h-yokokawa@aist.go.jp (H. Yokokawa).

0925-8388/$ – see front matter © 2007 Elsevier B.V. All rights reserved.
doi:10.1016/j.jallcom.2006.12.150

(1) Utilization of metal interconnects gives rise to new sources of degradations. One is the increasing resistance across oxide scales on metal interconnects on both the oxidative and the reductive sides [6,13]. Another is the cathode degradation caused by chromium oxide vapors emitted from the oxide scales. This is called chromium poisoning [14–16].
(2) Utilization of the thermodynamically less stable materials such as (La,Sr)FeO_3, (La,Sr)(Co,Fe)O_3 or rare-earth doped ceria [17,18].
(3) With decreasing temperature, the equilibria associated with chemical stabilities will be shifted. One typical example is the metal carbonate formation, which becomes favored at lower temperatures [19].
(4) With decreasing temperature, the electrochemical overpotential will increase when the same electrode materials are used. When the overpotential is one of the major driving forces for degradation, degradation should be enhanced even at low temperatures as it was observed for chromium poisoning [14,16].

These features suggest that there is a strong trade-off relation between the stability and the performance among SOFC perovskite cathode materials.

Fig. 1 schematically illustrates the materials issues associated with intermediate temperature solid oxide fuel cell cathodes. The evaporation of chromium from the oxide scales of metal interconnect has been intensively investigated by Hilpert and coworkers [20,21]. Reactions of evaporated chromium vapors with the cathodes to form Cr-containing compounds inside the cathode layers have been investigated previously [16]. For (La,Sr)MO_3 (M = Fe,Co) cathodes, a thin layer of rare earth doped ceria is used as diffusion barrier. Interdiffusion between YSZ and rare earth doped ceria is important, because the oxide-ion conductivity decreases significantly in the middle of the concentration range [22]. Thermodynamic [23] and interdiffusion [24] properties between YSZ and doped ceria are well investigated. When the three layers of cathode/doped ceria/YSZ are fabricated, the diffusion of Sr through the rare earth doped ceria from the cathode to YSZ becomes one of the key issues, because the strontium zirconate formation may take place at the ceria/YSZ interfaces not only during the fabrication but also during operation.

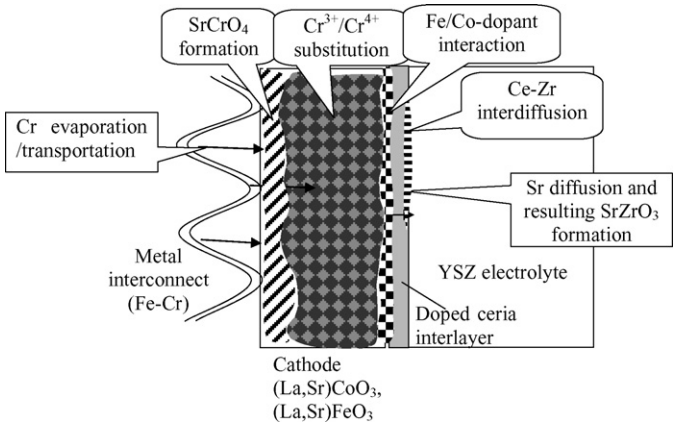

Fig. 1. Schematic view of the metal interconnect/cathode/interlayer/YSZ electrolyte multilayer structure for the intermediate temperature SOFCs.

In the present investigation, thermodynamic analyses will be made to extract the major characteristic features to distinguish the differences between (La,Sr)MnO_3, (La,Sr)FeO_3, and (La,Sr)CoO_3. The driving forces of the Sr diffusion through a doped ceria layer will also be examined in terms of the SrO activity and its gradient inside the layers. Several effects of changing the SrO-activity profile will be discussed. For this purpose, the perovskite/doped ceria interfaces will be characterized in terms of the chemical potential of the rare earth dopants. Finally, plausible effects of polarization will be examined in terms of the shift of equilibrium properties as a function of oxygen potential and in terms of the steepening of oxygen potential gradient.

2. Methods of thermodynamic analyses

2.1. Thermodynamic data

The main thermodynamic data of compounds are taken from the thermodynamic database MALT (Materials-oriented Little Thermodynamic database) for Windows [25]. Thermodynamic data of many perovskite oxides [26–28] were evaluated at an early stage of investigations focused on their reactions with YSZ [29,30]. Later detailed calorimetric measurements [31–34] have been performed and have essentially confirmed the majority of data for perovskite oxides.

The thermodynamic properties of rare earth doped ceria [23] as well as zirconia systems [35] were obtained by phase diagram calculations; interaction parameters for the ceria-based fluorite oxides were determined so as to reproduce the oxygen nonstoichiometry in pure ceria and doped ceria with the aid of the results from theoretical calculations [36,37]. These data were used to make attempts to correlate the electronic and proton behaviors with the thermodynamic activity of dopants and hosts [38]. Recent calorimetric results [33,39] are found to be essentially the same as the data used in the present investigation.

2.2. Methods of calculation and analysis in terms of valence stability and stabilization energy

The chemical equilibrium calculations were made by the GEM (Gibbs energy minimizer) program and the chemical potential diagrams were constructed by the CHD (chemical diagram) program in the MALT system [25].

To examine the driving force of the Sr diffusion, the SrO activity was calculated; those for perovskite materials were obtained using the CHD program, whereas the SrO activities in doped ceria and YSZ were calculated using the interaction parameters for the fluorite solid solutions in the SrO–ZrO_2 and the SrO–CeO_2 systems together with those for the $(RE_2O_3)_{0.5}$–MO_2 (RE = Rare Earth, M = Ce, Zr) systems.

In order to understand the physicochemical origins of the different features of the SrO activity in respective perovskite materials, analyses were also made in terms of the valence stability of the transition metal oxides and the stabilization energy of perovskite oxides (enthalpy change for formation of perovskite

oxides from their constituent oxides) [26,27]. The valence stability can be defined from the following valence change reaction in oxide systems:

$$MO_{n/2} + (1/4)O_2 = MO_{(n+1)/2} \quad (1)$$

$$\begin{aligned}\Delta[M^{n+};M^{(n+1)+}] &= \mu^\circ(MO_{(n+1)/2}) - \mu^\circ(MO_{n/2}) - (1/4)\,\mu(O_2) \\ &= \Delta h^\circ - T\Delta s^\circ - (1/4)RT \ln p(O_2) \quad (2)\end{aligned}$$

The stabilization energy of perovskite oxide AMO_3 can be defined in a similar manner:

$$MO_2 + AO = AMO_3 \quad (3)$$

$$\begin{aligned}\delta(AMO_3) &= \mu^\circ(AMO_3) - \mu^\circ(AO) - \mu^\circ(MO_2) \\ &= \Delta h^\circ - T\Delta s^\circ \quad (4)\end{aligned}$$

For the stabilization energy of the perovskite type oxides good correlations have been found with the tolerance factor that is defined as a measure for deviation from the ideal ionic packing in the perovskite lattice [26,27]. This suggests that the stabilization energies of $LaMO_3$ and $SrMO_3$ (M = Mn, Ti, etc.) exhibit only small differences depending on ionic radii, whereas the valence stability among the tetra-, the tri-, and the divalent oxides are quite different among Mn, Fe, and Co. These separated contributions make it possible to distinguish whether the difference in the SrO activity originates from the stabilization energy term or the valence stability term.

3. Results of thermodynamic calculations

3.1. SrO activity of perovskite cathode materials

Phase relations associated with (La,Sr)MnO_3, (La,Sr)FeO_3, and (La,Sr)CoO_3 were calculated at 1073 K. The SrO activities in these perovskite oxide are compared in Fig. 2 as a function of the Sr concentration. For (La,Sr)MnO_3 and (La,Sr)CoO_3, the stability region of the perovskite is limited by the presence of stable α-$SrMnO_3$ or $Sr_2Co_2O_5$. All perovskite oxides have a rather wide range of SrO activity even when the Sr concentration is fixed. This is related to the other coexisting phase. In (La,Sr)CoO_3, the high activities of SrO are associated with the equilibrium with (La,Sr)$_2CoO_4$, while the low activities of SrO are due to the equilibrium with CoO.

Fig. 2 clearly shows that the magnitude of the SrO activity is quite different among (La,Sr)MnO_3, (La,Sr)FeO_3, and (La,Sr)CoO_3. In order to understand the physicochemical origin of this difference, a consideration of the valence stability of the transition metal oxides and the stabilization energy are useful. Fig. 3 schematically explains how the SrO activity or the chemical potential of SrO is determined in those SrO–MO_x (M = Mn, Fe, Co) systems which have essentially the same stabilization energy, δ, but quite different valence stabilities, Δ. The valence stability of Fe^{4+} or Co^{4+} is weaker than that of Mn^{4+}; as a result, $SrCoO_3$ can coexist with CoO instead of CoO_2, which should be the constituent oxide of $SrCoO_3$. In Fig. 3, the SrO activity for the case in which $SrCoO_3$ coexists with CoO is shown as horizontal line. This should be compared with the low activity values in Fig. 2.

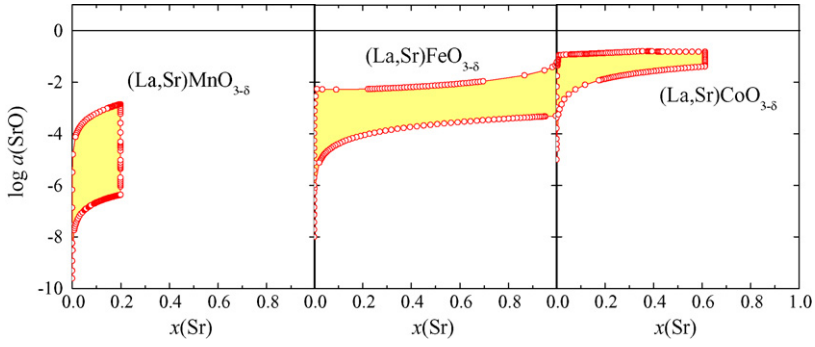

Fig. 2. The logarithmic activity of SrO in $(La_xSr_{1-x})MnO_3$, $(La_xSr_{1-x})FeO_3$, and $(La_xSr_{1-x})CoO_3$ at 1073 K.

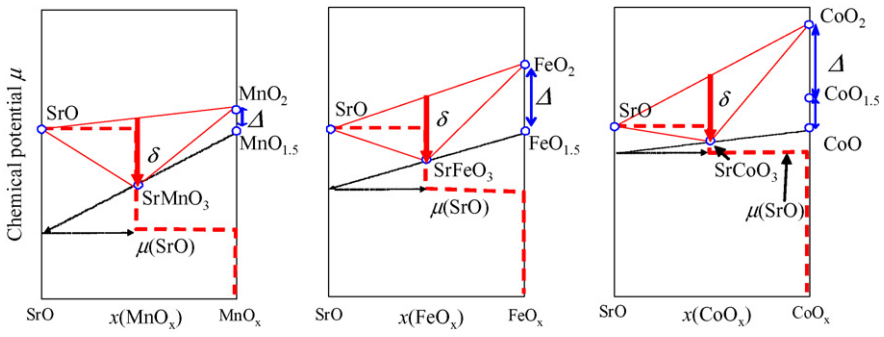

Fig. 3. Behavior of the chemical potential of SrO in the SrO–MO_x (M = Mn, Fe, Co) systems in relation to the valence stability, Δ, and the stabilization energy, δ.

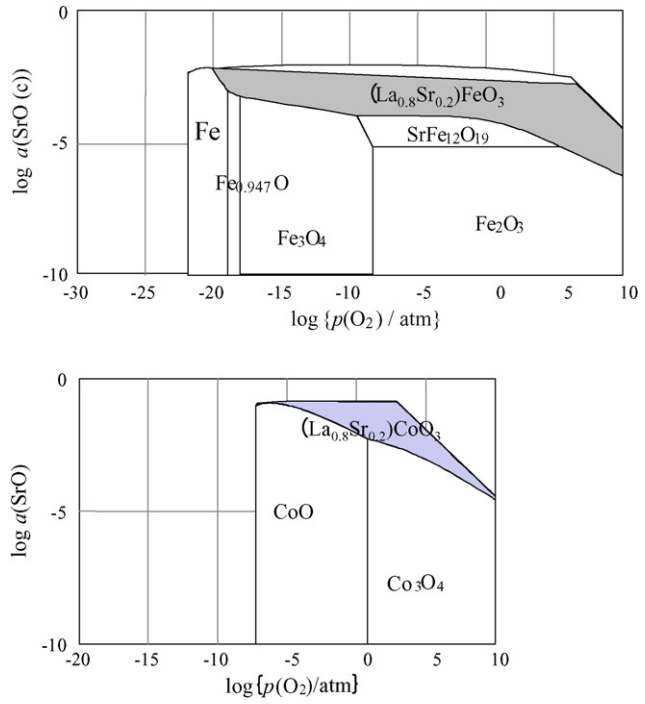

Fig. 4. The chemical potential diagram for the La–Fe–O and the La–Co–O systems at 1073 K under the condition of $a(LaMO_3) = 0.8$ (M = Fe, Co).

These differences in the SrO activity originating from the difference in valence stability can provide a reasonable basis of understanding those similarities of reactivity of perovskite cathodes with chromium vapors to that with YSZ which are summarized previously [16].

The SrO activity changes as functions of temperature and oxygen potential. The examples of $(La_{0.8}Sr_{0.2})FeO_3$ and $(La_{0.8}Sr_{0.2})CoO_3$ given in Fig. 4 were calculated under the condition of $a(LaMO_3) = 0.8$ (M = Fe, Co). The SrO activities within the stability area of perovskite increase slowly with decreasing oxygen potential in the La–Sr–Fe–O system but rapidly in the La–Sr–Co–O system. This can be also well understood in terms of the change in the valence stability as given by Eq. (2): The valence stability, Δ, changes through the partial pressure of oxygen. In the La–Sr–Co–O system, the stable binary oxide changes from Co_3O_4 to CoO, which also leads to an increase of the SrO activities.

3.2. Analyses on cathode/rare earth doped ceria/YSZ layers

From the high temperature chemistry point of view, the following materials issues related to the adoption of this ceria interlayer should be examined as indicated in Fig. 1;

(1) The less stable cathodes may chemically interact with doped ceria so that concentration change may happen at the interfaces.
(2) The doped ceria layer is thin so that diffusion through the layer becomes critical. In particular, there is a large driving force of forming $SrZrO_3$ between the cathodes and YSZ. This indicates the importance of diffusion of Sr through the doped ceria.

These issues will be examined in term of the SrO activity in the cathodes, doped ceria and YSZ below.

Fig. 5 compares the SrO activity among the cathode ((La,Sr)FeO_3 or (La,Sr)FeO_3), doped ceria and YSZ. The SrO activities in $(Ce_{0.8}Y_{0.2})O_{1.9}$ and $(Zr_{0.8}Y_{0.2})O_{1.9}$ were derived from phase diagram calculations [23,35]. The calculated SrO solubility in YSZ is quite small. Above the limiting value of $\log a(SrO) = -4.3$, $SrZrO_3$ will be precipitated. The SrO activities in $(La_{0.8}Sr_{0.2})FeO_3$ are higher than this critical value, which yields the driving force of the diffusion of Sr inside the doped ceria from the (La,Sr)FeO_3/(La,Sr)CoO_3 cathode to the YSZ electrolyte.

In $YO_{1.5}$ doped ceria, the SrO solubility was calculated to be 2 at.%, being limited by the formation of $SrCeO_3$. Fig. 5 shows the relation between the SrO solubility and the SrO activity in YDC. The diffusion flux is given by

$$J = cB\frac{d\mu}{dx} \tag{5}$$

where c is the concentration of diffusing species, B the mobility and $d\mu/dx$ is the gradient of the chemical potential of diffusing species. When the bulk diffusion is concerned, both the concentration and the driving force are important. This indicates that the higher the activities of SrO on the cathode side the more they enhance the solubility in the doped ceria. Thus, the SrO activity on the cathode side is important in providing a steeper chemical potential gradient and also in promoting the dissolution of SrO

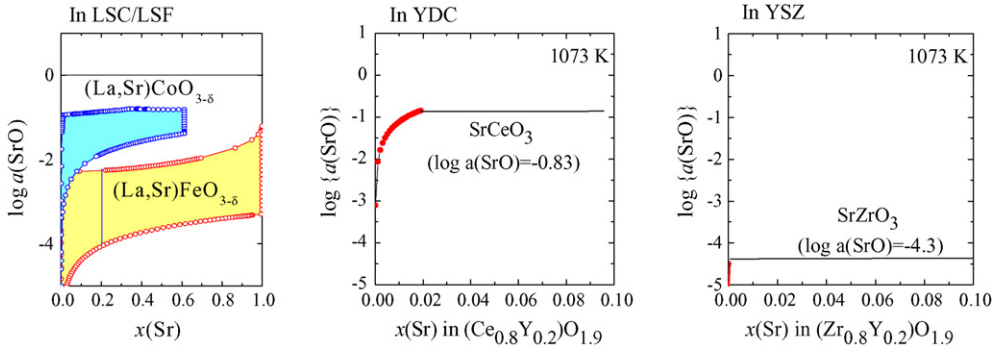

Fig. 5. Comparison of the logarithmic activity of SrO among the $(La_xSr_{1-x})FeO_3$/$(La_xSr_{1-x})CoO_3$, YDC($YO_{1.5}$ doped ceria) and YSZ($YO_{1.5}$ stabilized zirconia) at 1073 K.

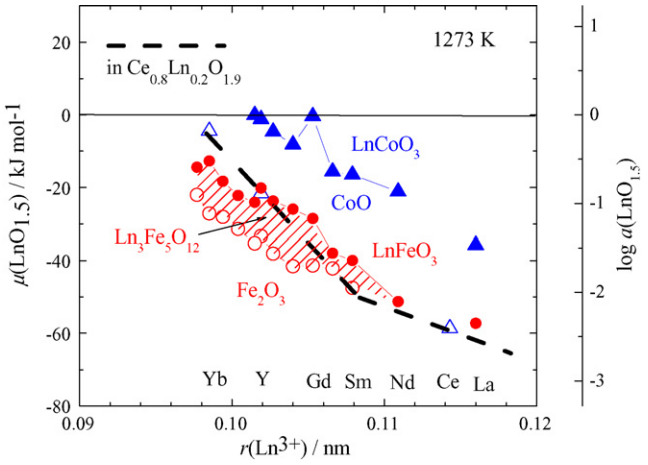

Fig. 6. Comparison of the chemical potential of rare earth oxides among $Ce_{0.8}Ln_{1.5}O_{1.9}$ and Ln–M–O (M = Fe, Co) system calculated for 1273 K and $p(O_2) = 0.2$ atm (for symbols, see text).

into ceria providing a larger flux of Sr through doped ceria. In (La,Sr)FeO_3, the activity of SrO is always lower than the critical value for the $SrCeO_3$ formation, indicating that there is no possibility of the $SrCeO_3$ formation at (La,Sr)FeO_3/doped ceria interfaces. On the other hand, in (La,Sr)CoO_3, there is some possibility of the $SrCeO_3$ formation because of the higher SrO activity in (La,Sr)CoO_3.

The SrO activity in those cathodes prepared at selected chemical compositions will be influenced by even a small change in concentrations. There are several possible mechanisms in which the concentrations of cathodes may change at the interfaces and therefore the SrO activity may also change.

3.2.1. *Interface reaction between perovskite and doped ceria*

When the cathode and the doped ceria are chemically interacting, the concentrations in the perovskite cathode may change thus leading to a change in SrO activity. Fig. 6 compares the chemical potentials of the rare earth oxide $LnO_{1.5}$ in ceria and in the Ln–M–O (M = Fe, Co) system at 1273 K and $p(O_2) = 0.2$ atm; the dashed line with open triangles are for rare earth doped ceria ($Ce_{0.8}Ln_{0.2}O_{1.9}$), Similarly, those in the Ln–Fe–O and the Ln–Co–O systems are given as circles and triangles, respectively. The chemical potentials of $LnO_{1.5}$ in the Ln–Fe–O systems are determined from the phase equilibria for $Ln_3Fe_5O_{12}/Fe_2O_3$ (open circles) and $LnFeO_3/Ln_3Fe_5O_{12}$ (solid circles) and $LnFeO_3/Fe_2O_3$ (Ln = Nd, La) (solid circles) by using the CHD program [25]. Fig. 6 indicates that the chemical potentials for the formation of $LnFeO_3$ are of the same order of magnitude as those of doped ceria ($Ce_{0.8}Ln_{0.2}O_{1.9}$). From these features, the following two processes can be expected:

(1) Interaction of perovskite oxides and dopants in doped ceria. Rare earth dopants can form the perovskite or the garnet phases at interfaces.
(2) Dissolution of the lanthanum component in perovskite into doped ceria.

Although the Sr component is not involved, the SrO activity depends sensitively on the above processes.

For the case of the Ln–Co–O system, the chemical potential of $LnO_{1.5}$ is not so much lowered by the formation of $LnCoO_3$ as apparent from Fig. 6. This indicates that the driving force for the formation of $LnCoO_3$ at the perovskite-doped ceria interface is quite small in the smaller rare earth dopants. Since the enthalpy change for formation of $LnCoO_3$ and $LnFeO_3$ is of about the same magnitude, the differences in chemical potential of $LnO_{1.5}$ given in Fig. 6 are again derived from the differences in the valence stability of Fe^{3+}/Fe^{2+} and of Co^{3+}/Co^{2+}.

3.2.2. *Effect of kinetic demixing*

When there is an oxygen potential gradient inside the cathodes, kinetic demixing may take place so that the SrO activity at the interface with doped ceria may change. This phenomenon depends on the difference in diffusion coefficients among cations in addition to the magnitude of the oxygen potential gradient. Usually, in the perovskite oxides, the A-site cations have the higher diffusivity than the B-site cations [40]. Even so, some perovskite oxides exhibit the same order of diffusivity like in (La,Sr)(Ga,Mg)O_3 [41] or even faster B-site cation diffusivity like in (La,Sr)FeO_3 [42]. In (La,Sr)(Co,Fe)O_3 and related perovskites, actual kinetic demixings have been reported recently [43,44] resulting in precipitation of Co/Fe-rich phases on the oxidative side. For (La,Sr)FeO_3 or (La,Sr)(Co,Fe)O_3, the cathode reactions are not restricted to the three-phase boundaries but take place mainly at the cathode surface. This means that an oxygen potential gap is developed across the cathode surface, whereas there is essentially no such potential gap at the interface between the cathode and the doped ceria. This implies that there is no significant effect of oxygen potential gradient on the changes in concentrations in (La,Sr)FeO_3 or (La,Sr)(Co,Fe)O_3, except for the three-phase-boundary area.

3.2.3. *Effects of polarization*

Effects of polarization can be considered in two ways. One is the shift of the oxygen potential inside the cathodes to the more reductive side. Another is the occurrence of oxygen potential gradients.

Fig. 4 shows that changes in the chemical potentials of SrO caused by the decrease in the oxygen potential are not so significant in the $(La_{0.8}Sr_{0.2})FeO_3$ cathode but rather significant in the $(La_{0.8}Sr_{0.2})CoO_3$ cathode. In a similar manner, the driving force for the $LnCoO_3$ formation at the cathode/doped ceria interface also decreases with decreasing oxygen potential, whereas no significant changes are expected for the formation of $Ln_3Fe_5O_{12}$ or the $LnFeO_3$. On the other hand, the kinetic demixing depends on the overpotentials, which lead to the oxygen potential gradients on the electrochemically active surfaces. For (La,Sr)FeO_3, diffusion of Fe has been found to be faster than La so that Fe ions are expected to move to the oxidative side causing enrichment of SrO or $LaO_{1.5}$ at the cathode/doped ceria interlayer interface.

By combining two effects, the following expectation can be derived:

(1) For (La,Sr)FeO_3 cathodes, effects of polarization will appear only as a result of kinetic demixing caused by the fast diffusion of Fe ion.
(2) For cathodes containing cobaltites such as (La,Sr)CoO_3 or (La,Sr)(Co,Fe)O_3, effects of polarization will appear in kinetic demixing and a shift in equilibrium caused by the small valence stability of Co^{3+} or Co^{4+}.

3.2.4. Effects of reactions with chromium vapors

When $SrCrO_4$ is formed as a reaction with chromium vapors, this means that the Sr component in the perovskite phase decreases being accompanied with the precipitation of transition metal oxide rich phases [16]. This leads to the lowering of the SrO activity in the perovskite phase. Similarly, the Cr^{3+}/Cr^{4+} substitution reactions also lead to such lowering. When this lowering is extended to the cathode-doped ceria interfaces, the reaction with chromium vapors decreases the driving force for the diffusion of Sr into the ceria–YSZ interface.

4. Discussions

The present results on the perovskite/doped ceria interface should be compared first with results of diffusion couple experiments [45,46] associated with perovskite cathodes and doped ceria, and then with the materials behavior under the operation of electrochemical cells. Finally, it should be investigated how they are correlated with the degradation behavior of cathodes operated with an interlayer of doped ceria. Such detailed comparisons are beyond the scope of the present manuscript. Here, we briefly describe our recent results of diffusion couples between (La,Sr)FeO_3/(La,Sr)CoO_3 and 20% Ln (La or Gd) doped ceria, $(Ce_{0.8}Ln_{0.2})O_{1.9}$ [46]. The main features of diffusion couple experiments can be summarized in comparison with the present results.

Essentially no diffusion of dopant or ceria into the perovskites was observed at temperatures of 1273–1473 K. This is consistent with the features given in Fig. 6; that is, the stabilization of $LaFeO_3$ or $LaCoO_3$ is strongest among the rare earth series so that there is little driving force for the rare earth dopant to diffuse into the perovskite lattice.

At the GDC (Gd doped ceria)–(La,Sr)CoO_3 interface, no reaction products were observed, whereas at the GDC–(La,Sr)FeO_3 interface, Gd–Fe–O double oxides were observed. This is again consistent with the features shown in Fig. 6, which indicates that the driving force for the formation of $GdCoO_3$ is essentially zero, whereas that of $GdFeO_3$ exists. Since the observed stoichiometric ratio between Gd and Fe was nearly unity this phase can be regarded as perovskite phase.

LDC (La doped ceria) formed island-like thin layers consisting of La and Fe or Co at the interfaces with (La,Sr)FeO_3 and (La,Sr)CoO_3, respectively. Again, the observed stoichiometric ratio between La and Fe/Co was nearly unity.

Whenever reaction products were formed at the interface, the new reaction products were formed on the doped ceria side, making a two-phase layer with a thickness of about 1 μm. In some cases, Sr diffusion took place beyond this two-phase region suggesting that the main diffusion path for Sr ions can be identified as grain boundaries.

Regarding the observations (3) and (4), Fig. 6 indicates that the activities of $LaO_{1.5}$ in $LaMO_3$ (M = Fe, Co) are higher than those in $(Ce_{0.8}La_{0.2})O_{1.9}$ leading to the expectation that the $LaO_{1.5}$ component in the perovskites will dissolve into the ceria phase to achieve an equilibrium between the $LaMO_3$ (M = Fe, Co) and (La,Ce)O_2 phase. Such driving forces are stronger in the (La,Sr)CoO_3/LDC couple as compared with the (La,Sr)FeO_3/LDC couple. As a result, thicker reaction products (about 2 μm) in the (La,Sr)CoO_3/LDC compared with thinner products (0.5 mm) in the (La,Sr)FeO_3/LDC couple are reasonably consistent with the thermodynamic situations.

Similarly, for the (La,Sr)FeO_3/GDC couple, the $LaO_{1.5}$ component will be dissolved into the ceria phase. However, in such a case, the chemical potential of slightly dissolved $LaO_{1.5}$ is quite low so that there is no chance to form $LaFeO_3$ in $(Ce_{0.8}Gd_{0.2})O_{1.9}$. Instead, $GdFeO_3$ or $Gd_3Fe_5O_{12}$ will be formed to coexist with the ceria phase. For the (La,Sr)CoO_3/GDC couple, no formation was observed. This is consistent with the fact that there is essentially no driving force of the formation of $GdCoO_3$ as shown in Fig. 6.

In any case, we can expect significant lowering in the chemical potential of $LaO_{1.5}$, providing a higher SrO chemical potential in the vicinity of the interfaces and promoting the SrO diffusion through the doped ceria.

5. Conclusions

The present investigation has revealed that in addition to the reactions with YSZ or with chromium vapors, the stability of the three-layer structure cathode/doped ceria/YSZ electrolyte is affected strongly by the valence stability of iron and cobalt oxides.

Plausible diffusion through the interlayer of doped ceria between (La,Sr)MO_3 (M = Fe, Co) and YSZ was analyzed in terms of the thermodynamic activity of SrO in (La,Sr)FeO_3 or (La,Sr)CoO_3, ceria and YSZ, and in terms of the solubility of SrO in $YO_{1.5}$ doped CeO_2. The formation of $SrZrO_3$ at the interfaces between ceria and YSZ depends on the diffusion of Sr and also on the driving force. The driving force for the formation of $SrZrO_3$ is stronger in (La,Sr)CoO_3 than in (La,Sr)FeO_3 because of the difference in the valence stability. The driving force of Sr diffusion depends on the chemical potentials of SrO at the cathode/doped ceria interfaces, which are in turn affected by cathode-doped ceria interactions or by kinetic decomposition. Both are enhanced by the cathode polarization.

Acknowledgement

A part of the present investigation was made by the support from the NEDO project on development for improving reliability of SOFC stacks/modules.

References

[1] S.C. Singhal, K. Kendall (Eds.), High Temperature Solid Oxide Fuel Cells Fundamentals, Design and Applications, Elsevier, 2003.
[2] H. Yokokawa, N. Sakai, in: W. Vielstich, A. Lamm, H.A. Gasteiger (Eds.), Handbook of Fuel Cells Fundamentals Technology and Application, vol. 1, John Wiley & Sons, 2003, pp. 219–266.
[3] S.C. Singhal, Solid Oxide Fuel Cells VI, PV 99-19, The Electrochemical Society, Inc., Pennington, NJ, USA, 1999, pp. 39–51.
[4] M. Yoshida, M. Suzuki, Proceedings of the 73rd Meeting of the Electrochem. Society Japan, April, 2006, p. 387.
[5] M. Takao, N. Komada, Proceedings of the Fuel Cell World, European Fuel Cell Forum, Lucerne, Switzerland, 2004, pp. 290–297.
[6] K. Hilpert, W.J. Quadakkers, L. Singheiser, in: W. Vielstich, A. Lamm, H.A. Gasteiger (Eds.), Handbook of Fuel Cells, vol. 4, John Wiley & Sons, 2003, pp. 1037–1054.
[7] H. Yokokawa, N. Sakai, T. Horita, K. Yamaji, M.E. Brito, Electrochemistry 73 (2005) 20–30;
H. Yokokawa, N. Sakai, T. Horita, K. Yamaji, M.E. Brito, Mater. Bull. 30 (8) (2005) 591–595.
[8] H. Yokokawa, T. Horita, in: S.C. Singhal, K. Kendall (Eds.), High Temperature Solid Oxide Fuel Cells Fundamentals, Design and Application, Elsevier, 2003, pp. 119–147.
[9] H. Yokokawa, N. Sakai, T. Kawada, M. Dokiya, J. Electrochem. Soc. 138 (1991) 2719.
[10] H. Yokokawa, Annu. Rev. Mater. Res. 33 (2003) 581–610.
[11] B.C.H. Steele, Solid State Ionics 134 (2000) 3–20.
[12] T. Kawada, K. Masuda, J. Suzuki, A. Kaimai, K. Kawamura, Y. Nigara, J. Mizusaki, H. Yugami, H. Arashi, N. Sakai, H. Yokokawa, Solid State Ionics 121 (1999) 271–279.
[13] T. Horita, K. Yamaji, T. Kato, N. Sakai, H. Yokokawa, J. Power Sources 131 (2004) 299–303.
[14] S. Taniguchi, M. Kadowaki, H. Kawamura, T. Yasuo, Y. Akiyama, Y. Miyake, T. Saitoh, J. Power Sources 55 (1995) 73–79;
S. Taniguchi, M. Kadowaki, T. Yasuo, Y. Akiyama, Y. Itoh, Y. Miyake, K. Nishio, Denki Kagaku 64 (6) (1996) 568–574.
[15] Y. Matsuzaki, I. Yasuda, Solid State Ionics 132 (2000) 271–278;
Y. Matsuzaki, I. Yasuda, J. Electrochem. Soc. 148 (2001) A126.
[16] H. Yokokawa, T. Horita, N. Sakai, K. Yamaji, M.E. Brito, Y.-P. Xiong, H. Kishimoto, Solid State Ionics 177 (2006) 3193–3198.
[17] A. Petric, P. Huang, F. Tietz, Solid State Ionics 135 (2000) 719–725.
[18] J.W. Stevenson, T.R. Armstrong, R.D. Carneim, L.R. Pederson, W.J. Weber, J. Electrochem. Soc. 143 (9) (1996) 2722–2729.
[19] H. Yokokawa, N. Sakai, T. Kawada, M. Dokiya, Solid State Ionics 52 (1992) 43.
[20] C. Gindorf, L. Singheiser, K. Hilpert, J. Phys. Chem. Solids 66 (2005) 384–387.
[21] K. Hilpert, D. Das, M. Miller, D.H. Peck, R. Weiss, J. Electrochem. Soc. 143 (1996) 3642–3647.
[22] H. Naito, H. Yugami, N. Sakai, H. Yokokawa, Solid State Ionics 135 (2000) 669–673.
[23] H. Yokokawa, N. Sakai, T. Horita, K. Yamaji, Y.-P. Xiong, T. Otake, H. Yugami, T. Kawada, J. Mizusaki, J. Phase Equilib. 22 (3) (2001) 331–338.
[24] K. Eguchi, N. Akasaka, H. Mitsuyasu, Y. Nonaka, Solid State Ionics 135 (2000) 589–594.
[25] The Thermodynamic Database MALT for Windows; Kagaku Gijutsu sha, http://www.kagaku.com/malt.
[26] H. Yokokawa, T. Kawada, M. Dokiya, J. Am. Ceram. Soc. 72 (1989) 152.
[27] H. Yokokawa, N. Sakai, T. Kawada, M. Dokiya, J. Solid State Chem. 94 (1991) 106.
[28] H. Yokokawa, N. Sakai, T. Kawada, M. Dokiya, J. Am. Ceram. Soc. 73 (1990) 649.
[29] H. Yokokawa, N. Sakai, T. Kawada, M. Dokiya, Denki Kagaku 57 (1989) 821;
H. Yokokawa, N. Sakai, T. Kawada, M. Dokiya, Denki Kagaku 57 (1989) 829;
H. Yokokawa, N. Sakai, T. Kawada, M. Dokiya, Denki Kagaku 58 (1990) 161.
[30] H. Yokokawa, in: Erich Kisi (Ed.), Zirconia Engineering Ceramics: Old Challenges—New Ideas, Trans Tech Publications, 1998, pp. 37–74.
[31] L. Rørmark, S. Stølen, K. Wiik, T. Grande, J. Solid State Chem. 163 (2002) 186–193.
[32] C. Laberty, A. Navrotsky, J. Solid State Chem. 145 (1999) 77–87.
[33] J. Cheng, A. Navrotsky, X.-D. Zhou, H.U. Anderson, J. Mater. Res. 20 (1) (2005) 191–200;
J. Cheng, A. Navrotsky, Chem. Mater. 17 (2005) 2197–2207.
[34] A. Navrotsky, P. Simomcic, H. Yokokawa, W. Chen, T. Lee, Faraday Discuss 134 (2007) 171–180.
[35] H. Yokokawa, N. Sakai, T. Kawada, M. Dokiya, Science and Technology of Zirconia V, Technomic Publishing Comp, Lancaster, Pennsylvania, 1993, pp. 59–68.
[36] L. Minervini, M.O. Zacate, R.W. Grimes, Solid State Ionics 116 (2000) 339–349.
[37] M.O. Zacate, L. Ninervini, D.J. Bradfield, R.W. Grimes, Solid State Ionics 128 (2000) 243–254.
[38] H. Yokokawa, T. Horita, N. Sakai, K. Yamaji, M.E. Brito, Y.-P. Xiong, H. Kishimoto, Solid State Ionics 177 (8) (2006) 1705–1714.
[39] M. Zinkevich, D. Djurovic, F. Aldinger, Proceedings of the Seventh European Solid Oxide Fuel Cell Forum, European Fuel Cell Forum, Lucerne, Switzerland, July 3–7, 2006.
[40] N. Sakai, K. Yamaji, T. Horita, Y.P. Xiong, H. Yokokawa, in: K.A. Gschneidner Jr., J.-C.G. Bünzli, V.K. Pecharsky (Eds.), Handbook on the Physics and Chemistry of Rare Earths, vol. 35, 2005, pp. 1–43.
[41] M. Martin, O. Schulz, in: B.V.R. Chowdari, H.-L. Yoo, G.M. Choi, J.-H. Lee (Eds.), Solid State Ionics: The Science and Technology of Ions in Motion, Word Scientific, Singapore, 2004, p. 787.
[42] I. Wærnhus, N. Sakai, H. Yokokawa, T. Grand, M.-A. Einarsrud, K. Wiik, Solid State Ionics, submitted for publication.
[43] H.L. Lein, K. Wiik, T. Grande, Solid State Ionics 177 (2006) 1587–1590.
[44] F. Iguchi, N. Sata, H. Yugami, H. Takamura, Solid State Ionics 177 (2006) 2281–2284.
[45] N. Sakai, T. Horita, K. Yamaji, M.E. Brito, H. Yokokawa, A. Kawakami, S. Matsuoka, N. Watanabe, A. Ueno, J. Electrochem. Soc. 153 (3) (2006) A621–A625.
[46] N. Sakai, H. Kishimoto, K. Yamaji, T. Horita, M.E. Brito, H. Yokokawa, Presented in 2006 Fall Meeting of the Electrochem. Society Japan, September 14, 2006.